Influence of Cluster-Support Interactions on Reactivity of Size-Selected Nb_xO_y Clusters

Miki Nakayama,[1] Meng Xue,[2] Wei An,[1] Ping Liu,[1] and Michael G. White[1, 2]

[1] *Chemistry Department, Brookhaven National Laboratory, Upton, NY 11973 (USA)*

[2] *Department of Chemistry, Stony Brook University, Stony Brook, NY 11794 (USA)*

Abstract

Size-selected niobium oxide nanoclusters (Nb_3O_5, Nb_3O_7, Nb_4O_7, and Nb_4O_{10}) were deposited at room temperature onto a Cu(111) surface and a thin film of Cu_2O on Cu(111), and their interfacial electronic interactions and reactivity toward water dissociation were examined. These clusters were specifically chosen to elucidate the effects of the oxidation state of the metal centers; Nb_3O_5 and Nb_4O_7 are the reduced counterparts of Nb_3O_7 and Nb_4O_{10}, respectively. From two-photon photoemission spectroscopy (2PPE) measurements, we found that the work function increases upon cluster adsorption in all cases, indicating a negative interfacial dipole moment with the positive end pointing into the surface. The amount of increase was greater for the clusters with more metal centers and higher oxidation state. Further analysis with DFT calculations of the clusters on Cu(111) indicated that the reduced clusters donate electrons to the substrate, indicating that the intrinsic cluster dipole moment makes a larger contribution to the overall interfacial dipole moment than charge transfer. X-ray photoelectron spectroscopy (XPS) measurements showed that the Nb atoms of Nb_3O_7 and Nb_4O_{10} are primarily Nb^{5+} on Cu(111), while for the reduced Nb_3O_5 and Nb_4O_7 clusters, a mixture of oxidation states were observed on Cu(111). Temperature programmed desorption (TPD) experiments with D_2O showed that water dissociation occurred on all systems except for the oxidized Nb_3O_7 and Nb_4O_{10} clusters on the Cu_2O film. A comparison of our XPS and TPD results suggests that Nb^{5+} cations associated with Nb=O terminal groups

act as Lewis acid sites which are key for water binding and subsequent dissociation. TPD measurements of 2-propanol dehydration also show that the clusters active toward water dissociation are indeed acidic. DFT calculations of water dissociation on Nb_3O_7 support our TPD results, but the use of bulk $Cu_2O(111)$ as a model for the Cu_2O film merits future scrutiny in terms of interfacial charge transfer. The combination of our experimental and theoretical results suggests that both Lewis acidity and metal reducibility are important for water dissociation.

Corresponding author contact information:

Michael G. White
Chemistry Department
Brookhaven National Laboratory
Upton NY 11974
Ph: (631) 344-4345
mgwhite@bnl.gov

Keywords:
water-gas-shift (or WGS), niobium oxide, Cu(111), Cu_2O, work function, water dissociation, 2-propanol dehydration, Lewis acid sites

1. Introduction

The water-gas-shift (WGS) reaction ($CO + H_2O \rightarrow CO_2 + H_2$) is an industrially important reaction with applications in hydrogen production and ammonia synthesis.[1-4] Copper-based catalysts are currently used for low-temperature WGS on an industrial scale, but they are not suited for mobile applications such as hydrogen fuel cells.[5] Studies of conventional catalysts, where Cu nanoparticles are supported on a metal oxide, have shown that the nature of the support has a significant impact on the catalytic activity, and that oxygen vacancies and electronic interactions between the Cu nanoparticles and the support play important roles.[6-7] In recent years, there has been an increased interest in inverse catalysts, where metal oxide nanoclusters are supported on a Cu substrate. These inverse catalysts serve as model systems to elucidate the role of oxides and oxygen vacancies, as oxygen vacancies can be stabilized and exposed on the small clusters.[8-9] Additionally, charged-particle probes can be used on these systems to study the interfacial electronic structure and charge transfer without major sample charging issues. In our previous work, we measured the work function shift before and after depositing several different metal oxide nanoclusters on Cu(111) using two-photon photoemission spectroscopy (2PPE) to investigate the effect of different metals, metal oxidation state, and cluster size on the interfacial dipole moment.[10]

Systematic studies have shown that catalysts involving easily reducible metal oxides, such as CeO_2 and TiO_2, are more active toward the WGS reaction.[8, 11-12] Ceria has received particular attention, especially with the finding that the CeO_x/Cu(111) inverse system exhibits higher WGS activity than both its conventional counterpart, Cu/CeO_2(111), and the traditional zinc oxide–supported Cu.[13] Niobium oxides are also known to be readily reducible with a wide range of stoichiometries and Nb oxidation states up to +5, e.g., NbO, NbO_2 and Nb_2O_5, which have found many applications in the field of heterogeneous catalysis,

especially as promoters or supports.[14-16] Moreover, Nb oxide is known to be a solid acid catalyst, acting as either a Lewis or Brønsted acid depending on the hydration conditions or the support in the case of supported Nb oxide.[14, 17] Supported Nb oxides have been studied in the form of overlayers on a high surface area oxide support such as alumina, silica, or titania, and their reactivity and acidity were investigated in relation to the Nb-O bond types and coordination at the surface.[18-19] Although Nb is not typically used as the main component of WGS catalysts, its incorporation into other systems have been shown to improve their WGS activity, either through structural effects or the interaction of Nb with water.[20-21] Also, lamellar niobates are known as photocatalysts for water dissociation,[22-23] which is considered to be the rate-limiting step for the WGS reaction on Cu.[24]

In order to obtain a fundamental understanding of the catalytic properties of Nb oxide with the ultimate goal of designing tailored catalysts, several groups have studied the properties and reactivity of Nb oxide nanoclusters in the gas phase.[25-29] Both theoretical and experimental methods have been used to determine the structures of some of the cationic, anionic, and neutral clusters; for example, $Nb_4O_{10}^-$ and $Nb_4O_{10}^+$ were found to have a cage structure.[26, 30] With regard to reactivity, Castleman and coworkers found that the cluster size and the degree of coordinative saturation affect the reactivity of the cationic clusters with *n*-butane, and that cationic clusters with a somewhat metal-rich character can abstract an oxygen atom from acetone.[25, 31-32] As for anionic clusters, Jackson and coworkers have reported that $Nb_xO_y^-$ undergo different reactions with methanol and ethanol depending on the oxidation state of Nb and the number of Nb-O double bonds.[29]

In our previous study, we showed that the combination of coverage-dependent 2PPE measurements and DFT calculations is a highly effective tool for understanding electron transfer at the cluster-support interface for a series of metal oxide nanoclusters on Cu(111).[10] Here, we first extend this study to Nb oxide nanoclusters. Specifically, we investigate the

effects of cluster size and metal oxidation state on the interfacial dipole by depositing fully oxidized Nb_3O_7 and Nb_4O_{10} and their "reduced" counterparts, Nb_3O_5 and Nb_4O_7, on Cu(111). (For the purposes of this study, we will be referring to Nb_3O_7 as fully oxidized, even though the average oxidation state of its Nb atoms is slightly below +5.) We also study the clusters deposited on a thin film of Cu_2O on Cu(111) as a case for mixed oxides, which better resemble realistic catalysts. Additionally, we explore the nanoclusters' activity toward water dissociation, the rate-limiting step of the WGS reaction, on both Cu(111) and Cu_2O films by conducting D_2O TPD experiments and detecting the D_2 molecules that desorb from the surface after recombination of the D atoms from dissociated D_2O. The oxidation states of the metal centers are monitored by XPS. We shed light on the mechanism of the water dissociation on these systems with the aid of DFT calculations and an analysis of the acidity of the systems using the dehydration of 2-propanol as an indicator.

2. Experimental and Theoretical Methods

2.1. Experimental Setup

The samples for this work were prepared in a cluster beam apparatus described in detail elsewhere.[33] The metal oxide clusters were generated by a DC magnetron sputtering source (Oxford Applied Research, NC200U-B), in which a metal (Nb) target was sputtered with a gas mixture of roughly 2% O_2 in Ar. The O_2 ratio could be tuned to optimize the yield of the specific cluster of interest. Helium was used as the cluster aggregation gas. The magnetron was typically operated at powers of about 100 W for the Nb oxide clusters. The generated cluster cations were passed through a quadrupole mass filter downstream, where a single cluster mass was selected by its mass-to-charge ratio so that only the cluster of interest for the experiment was deposited onto the substrate in the UHV analysis chamber (base pressure of $< 2 \times 10^{-10}$ Torr) at room temperature. An example of a mass distribution of the

Nb oxide clusters is shown in Figure 1. The cluster ion current on the crystal was monitored during deposition and integrated by a LabVIEW program to determine the number of clusters deposited. The flux of Nb oxide cluster ions on the substrate ranged from 10^{10} to 10^{11} clusters per cm^2 per second depending on cluster abundance and beam conditions. Typically, 1.5×10^{13} clusters were deposited for 2PPE and 2-propanol TPD experiments, and 3×10^{13} clusters for D_2O TPD experiments, resulting in an average coverage of about 0.15 and 0.3 ML, respectively, assuming a radius of 3 Å for the clusters and a radius of 3 mm for the deposition area. (The exact cluster area was determined from theoretical calculations described below.) For the Cu(111) surface which has an atom density of 1.8×10^{15} cm^{-2}, these coverages correspond to 0.03 and 0.06 clusters per Cu atom, respectively. The average cluster kinetic energy was also measured before and after deposition to ensure soft-landing conditions of less than 0.2 eV per atom.

Prior to deposition, the Cu(111) crystal (Princeton Scientific; 11 mm diameter, 2 mm thickness) was cleaned by two alternating cycles of Ar^+ sputtering (1 keV beam energy for 30 min) and annealing (700 K for 20 to 40 min). The crystal was heated resistively, and the temperature was measured by a K-type thermocouple fixed in a small hole on the edge of the crystal by high-temperature ceramic cement (Omegabond 600). The cleanliness of the substrate could be verified by AES and XPS. The Cu_2O/Cu(111) substrate was prepared by exposing the clean Cu(111) to 5×10^{-7} Torr of O_2 at 650 K for 20 min, and keeping it in the O_2 environment until it cooled down to 400 K. This preparation method results in a single layer Cu_2O film with the "44" structure.[34-37] The latter is composed of a O-Cu-O tri-layer structure that forms a honeycomb superstructure that resembles a distorted Cu_2O(111) surface with a unit cell roughly 44 times larger than the underlying Cu(111) surface.[34-38] The growth of the film is self-limiting to a single layer as shown by saturation of the oxygen signal in XPS and AES.[34, 37]

Work function measurements were made by single-color 2PPE experiments, described in detail in our previous work.[39] We used the third-harmonic radiation (~277 nm) generated from an ultrafast Ti:sapphire laser (Spectra-Physics Tsunami; 750-900 nm tunable, 100-fs pulse width). The laser pulses were p-polarized with an incident angle of 47.5˚ with respect to the surface normal. The beam was focused onto the sample surface by an achromatic lens for an estimated diameter of 0.25 mm. A bias voltage of –4.0 V was applied to the sample to improve the signal from electrons with low kinetic energy. Measurements were taken at 0.25- or 0.5-mm intervals along two perpendicular axes within the surface plane, crossing at the center of the sample surface. In order to obtain the coverage-dependent work function shifts, the measurements were taken at the exact same points before and after cluster deposition, and the local cluster coverage was determined by AES. A focused electron gun (SPECS, EQ 22/35) with a beam energy of 5 keV and beam size less than 0.2 mm was used for AES. The area of the O KLL Auger peak was measured at 0.5-mm intervals along two perpendicular directions, just as for 2PPE, to obtain the two-dimensional cluster distribution. Both our 2PPE work function shift and AES "line scans" resulted in distributions well described by Gaussian functions,[10] and they were ultimately indexed to each other by utilizing the fact that the maximum of all the Gaussian functions corresponds to the center point of cluster deposition, which we take to be the (0,0) position. We used a least-squares Gaussian fit to determine the center position and width of our 2PPE and AES data. A typical AES line scan had a FWHM of about 2 to 3 mm. Combining the cluster distribution information with the number of clusters deposited and the cluster adsorption structure obtained from DFT calculations described below, the local coverage at the point of each 2PPE measurement could be calculated. This allows us to obtain coverage-dependent work functions shifts from one sample. For both 2PPE and AES, a hemispherical electron energy

analyzer (SPECS, PHOIBOS 100) was used, and measurements were taken at room temperature.

Temperature-programmed desorption (TPD) experiments were conducted to investigate the activity of the oxide clusters on a Cu(111) or Cu_2O/Cu(111) surface toward water dissociation. A small amount of D_2O was held in a glass container connected to a gas inlet system, and was degassed by several freeze–pump–thaw cycles prior to the experiments. Dosing of the samples was performed by leaking a small volume of D_2O vapor (5 Torr) through a 50 μm (dia) aperture connected to the input side end of a stainless steel tube (6 mm dia) placed a few millimeters away from the sample. The D_2O was dosed at a sample temperature of 120 K and the exposure time was optimized to saturate the D_2 TPD signal associated with D_2O dissociation on the clusters. Prior to taking the TPD spectra, the sample was heated briefly to about 180-190 K to eliminate the background signal from the D_2O physisorbed onto the substrate so that the cluster-related peaks could be seen more clearly. For the TPD measurements, the sample was placed a few millimeters away from the entrance aperture of a quadrupole mass spectrometer (Hiden) which monitored multiple masses simultaneously. The heating rate for TPD measurements was 2 K/s.

The same setup was also used for 2-propanol TPD experiments. The 2-propanol was degassed by several freeze–pump–thaw cycles and the exposure conditions were optimized to produce roughly a monolayer of 2-propanol on the sample surface. For these experiments, we found the cluster-related peaks to be clearly visible without any pre-heating to eliminate the physisorption peak, unlike in the D_2O TPDs. We monitored the signals for 2-propanol at 45 amu and propene at 41 amu. The fact that the fragmentation pattern of 2-propanol contains mass 41 was taken into account in our analysis of the results.

XPS measurements were taken before and after the TPD measurements to determine the oxidation state of the metal in the clusters. The spectra were acquired using

unmonochromatized Al Kα radiation (1486.6 eV; SPECS, XR-50), and the same electron energy analyzer was used as mentioned above for 2PPE and AES. The Cu $2p_{3/2}$ binding energy at 932.6 eV was used as the reference energy for all spectra.[40] This is valid for our measurements on Cu_2O/Cu(111) as well because the Cu_2O is only a monolayer thick,[34] so most of the Cu signal comes from the bulk Cu(111) in the selvedge area. Moreover, the difference in the Cu $2p_{3/2}$ binding energy between Cu and Cu_2O is only about 0.1 eV.[41] The XPS peak fitting was carried out using the XPSPeak software (version 4.1) with a Shirley background. A small linear component was added to the Shirley background for the spectra of the clusters on Cu_2O/Cu(111) for a better fit. Gaussian-Lorentzian functions were used to fit the peaks, where the Gaussian percentage was allowed to vary between 70% and 90% but kept constant among the peaks within the same energy region. The FWHM was set to be the same within a spin-orbit doublet, and for fittings that require two sets of doublets, the FWHM of the two doublets were constrained so that they were within 0.3 eV of each other.

2.2. Theoretical Methods

The spin-polarized DFT calculations for this work were carried out with the Vienna *ab initio* simulation package (VASP),[42-44] where the generalized gradient approximation with the exchange-correlation functional of Perdew and Wang[45] was used. The calculations were performed within the projector-augmented wave method[46] using a plane-wave basis set with an energy cutoff of 400 eV. The 3d and 4s levels of Cu; 4p, 4d, and 5s levels of Nb; and the 2s and 2p levels of O were treated as valence states, while the levels below were kept frozen as core states. The partial occupancies were determined using the Gaussian smearing method with a thermal smearing of 0.05 eV for faster convergence.

Prior to calculating the adsorption structures on Cu(111), the gas phase structures of the Nb oxide clusters were optimized, starting from previously reported structures.[26] For these calculations, a single **k**-point was used and the clusters were put in a periodic cubic box

with an edge length of 15 Å. For Nb_4O_7, we also tried a planar structure, but it was found to be energetically unfavorable compared to the cage structure. Once the gas phase structures were optimized, the clusters were deposited on a 4-layer slab of Cu(111) with a (5×5) supercell geometry and 20 Å of vacuum on top so that the clusters would not interact with the bottom of the slab in the neighboring repeating unit. The Brillouin zone was sampled by a 3×3×1 Monkhorst-Pack grid of special **k**-points.[47] During the calculations, the bottom two layers of the Cu(111) slab were fixed in their bulk positions, while the top two layers along with the cluster were allowed to relax. Once the optimized adsorption structures were calculated, we used the spatial descriptors model in Materials Studio software, which takes the van der Waals radii into account, to obtain the cluster shadow area in the plane of the Cu(111) surface for the analysis of our 2PPE data. A Bader analysis program[48-49] was employed to investigate the electron transfer between the cluster and the support, as well as the charges on each atom.

For a more detailed analysis of water dissociation on Nb_3O_7, we placed the cluster on top of a *p*(5×5) three-layer slab of Cu (111) surface and a *p*(2×2) nine-layer (O-Cu-O) slab of Cu_2O (111) surface with a 22 Å vacuum between the slabs. In these calculations, all atoms were allowed to relax except those of the bottom two layers in the Cu(111) slab and the bottom six layers in Cu_2O(111) slab, which were fixed at their optimized bulk positions (3.634 Å for *fcc* Cu, and 4.271 Å for cubic Cu_2O bulk). The conjugate gradient algorithm was used in optimization, allowing the convergence of 10^{-4} eV in total energy and 0.02 eV/Å in Hellmann-Feynman force on each atom. The Brillouin-zone integration was sampled by the same Monkhorst-Pack grid as above. The water adsorption energy was defined as E_{ads} = $E(H_2O/Nb_3O_7/substrate) - E(Nb_3O_7/substrate) - E(H_2O)$, where the right hand terms stood for the total energy of water adsorbed on a supported Nb_3O_7, a supported Nb_3O_7, and a water molecule in gas phase, respectively. The climbing-image nudged elastic band (CI-NEB)

method [50-51] was used to locate the transition state structure along the minimum-energy pathway (MEP) for water dissociation.

3. Results and Discussion

3.1. Cluster-Support Interactions

3.1.A. Interfacial Dipoles from Work Function Measurements

Representative subsets of the 2PPE spectra that we have obtained at different niobium oxide cluster coverages on Cu(111) and Cu_2O/Cu(111) are shown in Figure 2. The spectra are plotted as a function of final state energy with respect to the Fermi level so that the work function can be determined directly from the low-energy cutoff position.[39, 52] In addition to the secondary electron peak, we also observe a feature associated with the Cu 3d band centered near 6.7 eV, and an asymmetric peak around 8.5 eV which corresponds to a mixture of the surface state (SS) and the unoccupied first image state (IS_1) located 0.4 and 0.8 eV below the Fermi level (E_F), respectively.[10, 53] The asymmetric peak is quenched as clusters are deposited onto the surface, and also when the oxide film is formed. Additionally, a feature attributed to an unoccupied state appears at around 7.4 eV for the Cu_2O/Cu(111) system.[54] In this study, we are interested in the work function, and therefore focus on the low-energy cutoff position. It can be seen qualitatively from Figure 2 that the cutoff position shifts upwards as more clusters are deposited, meaning the work function increases with increasing cluster coverage.

The values of the work function were obtained by differentiating the 2PPE spectra and determining the inflection point of the low energy onset. The work function shifts, $\Delta\Phi$, were calculated by subtracting the work function of the clean Cu(111) or Cu_2O/Cu(111) substrate from that of the cluster-deposited system at the exact same location. The local cluster coverage at each position on the surface was derived from the experimentally

measured spatial distribution of the clusters and knowledge of the cluster size. The latter is obtained from the DFT-optimized cluster adsorption structures shown in Figure 3. We performed DFT calculations only on Cu(111) because calculations on the Cu_2O/Cu(111) thin film structure require a larger unit cell[34] and thereby incur significantly more computational cost. Sample calculations of Nb_3O_7 and Nb_3O_5 on Cu_2O(111) have shown that the area the clusters occupy on the surface is fairly similar on the oxide compared to on Cu(111) (see Figure S1 in SI), and therefore we use the same cluster area obtained on Cu(111) to derive the local coverage on Cu_2O/Cu(111). The resulting work function shifts versus coverage of the niobium oxide clusters are shown in Figure 4.

In order to obtain a quantitative understanding of our work function results, we apply the classic Topping model[55] to our data, which relates the work function shift to the interfacial dipole. We use a variant of the Topping model for immobile adsorbates that involves a constant δ related to the geometry and mobility of the adsorbates.[56] Here, we set δ equal to $\theta^{-0.5}$, where θ is the cluster coverage, based on the lattice gas model for randomly distributed adsorbates, appropriate for our experimental conditions.[10, 57] The resulting Topping equation written in terms of θ and cluster area (A) is

$$\Delta\Phi = \frac{e\mu\theta}{A\varepsilon_0}\left(1 + \frac{9\alpha\theta}{4\pi A^{3/2}}\right)^{-1} \quad (1),$$

where e is the electron charge, ε_0 is the vacuum permittivity, μ is the surface dipole moment for a single cluster, and α is the cluster polarizability. This equation tells us that the work function shift is proportional to the coverage at low coverage, but it starts to plateau as the coverage increases. This is because of depolarization effects caused by dipole-dipole repulsions.

The results of the least-squares fitting of our work function data to equation (1) where μ and α are the fitting parameters are shown as solid lines in Figure 4. The value of α was constrained to be greater than or equal to zero. The calculated values of μ from the Topping

model fits are given in Table 1. For all of the clusters studied, $\Delta\Phi$ is positive and results in a negative interfacial dipole (the Topping model uses the physics convention of the dipole direction, pointing from negative to positive). If we assume that the interfacial dipole arises from charge transfer alone, then a negative dipole implies charge transfer from the support to the cluster. In our previous study of surface dipoles for W and Mo oxide clusters deposited on Cu(111), we found a general correlation between the magnitude of the surface dipole and the work function of the bulk oxide, even for bulk reduced oxides.[10] In the case of bulk Nb oxides, the measured work function values strongly depend on the Nb oxide phase (e.g., Nb_2O_5, NbO_2, NbO) and state of reduction with a maximum of ~5.2 eV for Nb_2O_5 and near continuous decrease to 4.2 eV for polycrystalline Nb metal.[58] The work function for both Cu(111) and the Cu_2O/Cu(111) thin film is 4.85 eV,[54] so that charge transfer to the cluster should occur for the fully oxidized Nb clusters, but may actually reverse for clusters with smaller oxygen-to-Nb atom ratios. These expectations are consistent with the observation of negative surface dipoles and with the fact that for clusters with the same number of Nb atoms, the reduced cluster results in a smaller interfacial dipole moment (Nb_3O_5 vs. Nb_3O_7, Nb_4O_7 vs. Nb_4O_{10}). This also follows the intuition that the reduced metal centers cannot accommodate as much charge from the support as the fully oxidized metals. We also note that for the reduced or fully oxidized clusters, the cluster with more metal centers (Nb_3O_5 vs. Nb_4O_7 and Nb_3O_7 vs. Nb_4O_{10}) results in a larger interfacial dipole moment. This trend is reasonable since the more metal cations there are in the cluster, the more charge the cluster can accommodate from the support. Both of these trends were observed in our previous studies of W and Mo oxide clusters on Cu(111).[10]

The attribution of the observed trends in surface dipole (Figure 4 and Table 1) to interfacial charge transfer assumes that the contribution from the intrinsic dipole of the cluster is small by comparison.[10] To gain insight into the contribution of charge transfer to the

interfacial dipole, we performed Bader charge analyses on the clusters on Cu(111). Based on the positive work function shifts observed in the 2PPE experiments for all the clusters, one may expect electrons to be transferred from the Cu substrate to the clusters in all cases. However, the results of the Bader analysis, shown in Table 1, indicate that the direction of charge transfer is different for the fully oxidized and reduced clusters; electrons are transferred from Cu(111) to the fully oxidized clusters, but the reduced clusters are *donating* electrons to Cu(111). As noted above, this is consistent with smaller work functions for bulk Nb oxide phases with lower oxygen content than Nb_2O_5. This means that for the reduced clusters, the overall interfacial dipole does not reflect the direction of charge transfer but rather the intrinsic dipole of the clusters. Looking at the calculated cluster structures in Figure 3, the reduced clusters on Cu(111) indeed have less O-Cu interactions compared to their fully oxidized counterparts, and/or they have more oxygen atoms above the plane of the Nb atoms (above the center of the cage for the clusters with four Nb atoms) than below. As a result, the reduced clusters are expected to have intrinsic dipoles which could mask the charge transfer contribution to the overall surface dipole.[10]

Although the trends regarding cluster size and metal oxidation state are shared between the clusters on Cu_2O/Cu(111) and on Cu(111), we see from Figure 4 that the work function shift behavior is very different between the two systems. On Cu(111), the work function shift increases linearly or quasi-linearly with cluster coverage for all clusters except Nb_4O_{10}, for which a slight curvature is observed due to depolarization with increasing coverage. In contrast, the curvature due to depolarization is much more apparent for all the clusters on Cu_2O/Cu(111), and the magnitudes of the work function shifts are much greater, resulting in greater dipole magnitudes (see Table S1 in SI for experimentally derived values of μ). The greater dipole magnitudes may reflect charge redistribution induced by cluster–oxide binding as well as local restructuring of the Cu_2O film that modifies the electronic

properties of the Cu_2O-Cu interface. In particular, thin dielectric films on metals are known to introduce work function shifts as a result of charge transfer via chemical interactions as well as "compression" effects resulting from decreased penetration of the metal's electrons into the vacuum as a result of the barrier introduced by the thin dielectric film.[59] Charge transfer is generally from the metal to the oxide film which increases the work function, whereas compression effects depend mainly on the distance between the oxide film and the metal surface and generally result in a decrease in the metal work function. As noted above, the work functions of both the bare Cu(111) and the Cu_2O/Cu(111) surfaces are essentially identical, suggesting that the these two contributions cancel each other. This balance is likely to be disrupted by electronic interactions with the deposited clusters, so that the work function shifts now include contributions from cluster dipole, charge transfer and compressive effects. The presence of the oxide film could also act as a spacer layer that simply increases the distance of charge separation, i.e., distance between the clusters and metal surface, which would also have the effect of increasing the surface dipole. Overall, the large change in surface dipoles for the Nb_xO_y clusters deposited on the Cu_2O/Cu(111) surface clearly suggest strong interactions and charge redistribution at the cluster-oxide interface.

3.1.B. Nb Atom Charge State from XPS Core Level Spectra

Significant changes in the Nb 3d XPS spectra were observed when the clusters were deposited on the Cu_2O film compared to on bare Cu(111). The spectra are shown in Figure 5 along with their fits. In fitting the Nb 3d region, the area of the $3d_{5/2}$ peak was assumed to be 1.5 times that of the $3d_{3/2}$ peak, i.e., the relative degeneracy of the spin-orbit components. We first fit the spectrum of Nb_4O_{10} on Cu(111) to one spin-orbit doublet since it should only consist of Nb in the +5 oxidation state. This resulted in $3d_{3/2}$ and $3d_{5/2}$ binding energies of 210.6 and 207.9 eV, respectively, with a FWHM of 2.3 eV. The binding energy positions are slightly higher than those typically reported for the fully oxidized Nb^{5+},[60-61] but this is most

likely because we are making measurements on predominantly isolated nanoclusters rather than on bulk oxides or thick oxide films, resulting in less core-hole screening.[62] Once the binding energies and FWHM of Nb^{5+} were determined, we fit the Nb 3d peaks of the remaining systems to a combination of the Nb^{5+} doublet and another doublet, making sure that the FWHM did not exceed 2.5 eV and that the doublet separation was in the range of 2.6 to 2.8 eV.[60, 63] The binding energies and FWHM of the fitted curves are given in Table 2. The binding energies of 209.2-209.6 and 206.4-206.8 eV are assigned to $3d_{3/2}$ and $3d_{5/2}$ of Nb^{4+}, respectively, and 207.9 and 205.2-205.3 eV are assigned to $3d_{3/2}$ and $3d_{5/2}$ of Nb^{3+}, respectively, based on previous literature where the oxidation state of Nb and the Nb 3d binding energies were shown to be in a linear relationship.[60, 64]

It can be seen from Figure 5b and Table 2 that the fully oxidized Nb_3O_7 consists mainly of Nb^{5+} with a small amount of Nb^{4+} on Cu(111), but on the Cu_2O film, the composition becomes mostly Nb^{4+} with a small amount of Nb^{5+}. A similar behavior is observed for Nb_4O_{10}; it becomes mostly Nb^{4+} on Cu_2O/Cu(111) (Figure 5d). These results are surprising since they suggest that the clusters on the Cu_2O oxide film are "reduced" compared to on the Cu(111) surface. The larger work function shifts measured by 2PPE are consistent with more charge transfer to the clusters on the Cu_2O film (see Figure 4), but it is also possible that the observed shifts in the Nb 3d binding energies are influenced by final state effects in the photoemission process. Previous studies have shown that electrons can be transferred (via tunneling) to nanoclusters supported on an ultrathin metal oxide film grown on a metal substrate,[65-68] and Torelli et al. noted that this negative charge accumulation on the cluster could provide more efficient screening of the core hole.[69] Although we are currently unable to quantify the contributions of differential final state effects to the observed shifts in Nb 3d binding energies, our results clearly indicate that the clusters experience a very

different electronic environment when they are deposited on Cu_2O/Cu(111) compared to on Cu(111).

As for the reduced Nb_3O_5 and Nb_4O_7 clusters deposited on Cu(111), the XPS results indicate that the Nb atoms exist in two different oxidation states, assigned to Nb^{5+} and Nb^{3+} (Figures 5a and 5c). This is consistent with our DFT-calculated structures (Figures 3a and 3c) which exhibit two inequivalent Nb sites. Nb_3O_5 has two Nb atoms which are bonded to terminal oxygen atoms, and one Nb bonded only to bridging oxygen atoms. According to the Bader charge analysis, the Nb atoms involved in terminal oxygen bonding have a smaller total electron count (-0.6e) than the Nb atom participating in bridge oxygen bonding only, and are therefore more "oxidized." Similarly, the Nb atom bound to a terminal oxygen at the top of the cage in the Nb_4O_7 cluster has a smaller electron count (-0.5e) compared to the other Nb atoms in contact with the Cu(111) surface and bonded to bridging oxygen atoms only.

When the reduced clusters are deposited on the Cu_2O film, Nb^{3+} disappears and a mixture of Nb^{5+} and Nb^{4+} is observed. Here, initial state effects should be dominant, since increased screening due to electron transfer through the film would not account for the loss of the Nb^{3+} oxidation state. The changes in Nb oxidation states indicated by XPS suggest that some of the Nb atoms in the reduced clusters experience a change in coordination when deposited on the Cu_2O thin film compared to on Cu(111). The latter could result from additional bonding interactions between Nb atoms of the cluster with lattice oxygen atoms in the Cu_2O film.

Another interesting observation that can be made from our XPS results is that in general, the spectra of the clusters on Cu_2O/Cu(111) could be fit with curves with smaller FWHM than on Cu(111) (Table 2). A smaller FWHM suggests that there is less variation in cluster adsorption sites and geometries.[69] A more ordered distribution of clusters on

Cu_2O/Cu(111) as compared to the flat Cu(111) surface would be consistent with a higher surface corrugation of the oxide film.

3.2. Reactivity toward Water Dissociation

We studied the clusters' reactivity toward water dissociation by conducting D_2O TPD experiments and detecting the D_2 molecules that desorb from the surface via recombination of the D atoms from D_2O dissociation. We simultaneously monitored the D_2O signal as well. The results for the niobium oxide clusters are shown in Figure 6. We see that on Cu(111), both the fully oxidized and reduced clusters are active (Figure 6a). They all show a fairly broad peak with an onset temperature of about 300 to 310 K and a peak temperature between 370 and 395 K. All of the samples remained active for at least three repeated TPD runs, and the peak intensity increased after the first run as seen for the Nb_3O_7 cluster on Cu(111) (Figure 6c). On Cu_2O/Cu(111) however, only the reduced clusters were active toward water dissociation (Figure 6b). The peak characteristics of the reduced clusters were similar to those on Cu(111) with an onset temperature of about 310 K and a peak temperature of about 375 K. As with the clusters on Cu(111), the reduced clusters on Cu_2O/Cu(111) remained active for multiple TPD runs, and an increase in peak intensity was observed after the first run. The simultaneous D_2O TPD for the Nb_3O_7 cluster on Cu(111) exhibits a broad decreasing background from D_2O physisorbed on the substrate and a shoulder appears above 300 K after the first run (Figure 6d). Similar D_2 and D_2O desorption spectra were also observed for the other clusters deposited on Cu(111) studied in this work (see Figures S2 and S3 in SI). The shoulder in the D_2O TPD was not observed for the clusters on Cu_2O/Cu(111). We also monitored the Nb oxidation state before and after the TPD experiments using XPS, but found no significant shifts in binding energy (see Figure S4 and Table S2 in SI).

To investigate the possibility of thermal effects, e.g. cluster restructuring or agglomeration, we also performed TPD and XPS experiments after heating the as-deposited clusters on Cu(111) to 500 K. TPD results for Nb_3O_5 on Cu(111) (Figures S2 in SI) show that pre-heating does not lead to substantial changes in the D_2 and D_2O TPD traces after the first water dose and is unlikely to be responsible for the increase in D_2 desorption yield observed for the 2nd and 3rd TPD cycles. Moreover, the XPS data (Figure S5 in SI) also show that pre-heating the deposited clusters prior to the first TPD run does not alter the Nb 3d XPS spectrum, nor is it substantially modified in the subsequent 2nd and 3rd TPD runs. Although some thermally induced modifications of the clusters may occur during the TPD runs, these results suggest that heating alone (< 500 K) does not substantially change the chemical or electronic properties of the deposited Nb_xO_y clusters.

From the XPS results in Figure 5, we notice that for all of the clusters that are active toward water dissociation, the Nb 3d spectra contain a significant contribution from Nb^{5+}, suggesting that Nb^{5+} plays a key role in water dissociation. The fully oxidized clusters on Cu_2O/Cu(111), which are inactive for water dissociation, display a downward shift in Nb 3d binding energy, indicating that the Nb atoms are in a different, potentially more electron-rich environment as noted earlier. We note that from our calculated structures and Bader charge analyses, the most highly "oxidized" Nb atoms in the clusters on Cu(111) are involved in double bonds with a terminal oxygen atom. It is well known that Nb^{5+} cations associated with Nb=O double bonds are Lewis acid sites, and therefore can easily bind water.[14, 70] These terminal Nb=O groups are found in distorted NbO_6 octahedra of supported Nb_2O_5 catalysts,[71] and on catalytically active tetrahedrally coordinated Nb atoms in zeolites,[72] as well as in Nb oxide nanocluster cations in the gas phase.[26] Our calculated bond lengths between a Nb atom and a terminal oxygen atom not interacting with the Cu substrate are 1.74 Å for Nb_3O_7 (**1**) and 1.75 Å for all others, which match the reported Nb=O bond length values between 1.71

and 1.76 Å.[71] If the terminal oxygen is also interacting with the Cu substrate, the bond lengths increase slightly (1.81-1.82 Å for Nb_3O_5 (**2**), 1.80 Å for Nb_3O_7 (**2**), and 1.85-1.87 Å for Nb_4O_{10}), but they are still shorter than Nb-O single bonds, and therefore we expect the Nb atoms in this case to be weak Lewis acids.

Xie et al. studied the adsorption of water on Nb oxide thin films on Pt(111), and found that water molecules stay intact on fully oxidized Nb_2O_5 thin films but dissociate on Ar^+ bombarded Nb_2O_5 thin films at room temperature.[73] The Nb_2O_5 thin film was found to contain Nb=O terminal groups, which means that the presence of Nb=O terminal groups alone does not guarantee water dissociation. The authors suggest that the water dissociation may be induced by either the reduced Nb cations or the distortion of the crystal structure adjacent to oxygen vacancies created by the Ar^+ bombardment. Our XPS results suggest that it is the latter. Initially, the Nb_2O_5 film consists of distorted NbO_6 octahedra, but it is plausible that the Ar^+ bombardment creates under-coordinated Nb^{5+} sites (less than 6-fold coordinated) with a Nb=O terminal group, and that these sites are responsible for water dissociation. For example, Nb_2O_5 supported on SiO_2 is reported to consist of dispersed NbO_4 species with one Nb=O terminal group,[74] and all the Nb=O groups in our nanoclusters are either in this tetrahedral coordination or 5-fold coordinated (see Figure 3). The adsorption of water on under-coordinated sites in metal oxides is a generally accepted phenomenon,[75] and water adsorption specifically on Nb^{5+} sites has also been suggested in previous literature.[70, 72]

From the correlation between the XPS and TPD results discussed above, we propose that the water molecules initially adsorb and dissociate on Nb^{5+} cation sites which are doubly bonded to a terminal oxygen atom, i.e., Lewis acid sites. Water dissociation results in the formation of two OH groups which, according to the DFT calculations described below, are located at the original terminal oxygen site and a nearby bridging oxygen. Bridging Nb-OH-Nb groups reportedly act as strong Brønsted acids,[76] so additional water molecules could

adsorb at these sites once they are formed.[70] According to Andersson et al., the formation of stable H_2O-OH complexes involving multiple water molecules leads to water dissociation on not only Cu(110), which they studied, but metal surfaces in general.[77] In our nanocluster systems, the bridging OH groups would be at the cluster-substrate interface in most cases, and therefore could act as sites where water dissociation occurs. The possibility of water dissociation at both Lewis and Brønsted acid sites on the clusters provides a plausible explanation of the TPD results where the activity (Figure 6c) and water adsorption profile (Figure 6d) change after the first reaction cycle. In the initial TPD run, water adsorption and dissociation occur at the Nb=O sites leading to the formation of bridging Nb-OH-Nb which promote further water dissociation via H_2O-OH complexes at the Cu(111) interface. The bridging OH groups on the clusters are expected to be stable at the highest temperature reached in the TPD experiments (~475 K),[73] so that the hydrogen recombination product (D_2) most likely originates from water dissociation via the H_2O-OH complexes. The remaining oxygen from dissociated water is most likely in the form of O-adatoms on the Cu surface. We attribute the broad shoulder near 300 K in the water TPD spectra for the second and third runs (Figure 6d) to the presence of these O-adatoms. This assignment is based on previous studies which showed that water TPD from Cu surfaces pre-covered with oxygen exhibited additional peaks at higher temperature associated with H_2O-O(H) complexes and OH recombination.[75, 78-81] Moreover, additional TPD measurements (not shown) on the Cu(111) surface with a low coverage of oxygen atoms[82] exhibited increased water desorption and a broad desorption feature in the 260-350 K temperature range similar to that in Figure 6d. These results support the formation of O-adatoms as a likely product of water dissociation on the Nb_xO_y/Cu(111) surfaces.

The fully oxidized clusters on Cu_2O/Cu(111) are inactive with respect to water dissociation presumably because the Nb=O Lewis acid sites have disappeared through

interactions with the oxide film. The Nb atoms may interact with the oxygen anions, which would reduce the acidity of the Nb cation, and/or the terminal oxygen atoms on the cluster may be interacting with Cu atoms in the film which would result in the loss of Nb=O double bonds. Such strong cluster-support interactions can lead to substantial distortions of both the cluster and oxide surface as has been reported for W_3O_9 on a Cu-O (2×1) surface.[83] The loss of Nb=O sites and cluster deformation on Cu_2O can be clearly seen by comparing the DFT calculated adsorption structures of Nb_3O_5 on Cu(111) (Figure 3b) versus the bulk terminated Cu_2O(111) surface used as a model for the thin film structure (see Figure S1a in SI).

3.3. Dehydration of 2-Propanol

In order to provide support for our proposed water dissociation mechanism based on the acidity of the Nb clusters, we conducted 2-propanol TPD experiments on the reduced Nb_3O_5 and fully oxidized Nb_3O_7 clusters on Cu_2O/Cu(111). The decomposition of 2-propanol on solid metal oxide catalysts is commonly used to investigate the acid-base properties of the catalysts. In particular, the dehydration of 2-propanol to propene is regarded as an indicator of the acidity of the surface.[84-85] Recently, the dehydration of 2-propanol was observed on W_3O_9 clusters on TiO_2(110) and attributed to strong Lewis acid sites of W^{6+} with oxygen double bonds,[86] and on a graphene monolayer on Pt(111), W_3O_9 showed a higher reactivity for dehydration compared to Mo_3O_9 because W^{6+} is a stronger Lewis acid than Mo^{6+}.[87]

The results of our 2-propanol TPD experiments are shown in Figure 7. It is clear from Figure 7a that Nb_3O_5 is active for dehydration of 2-propanol while Nb_3O_7 is not; there is a propene peak centered around 460 K for Nb_3O_5, but no such peak is observed for Nb_3O_7. These results indicate that Nb_3O_5 is acidic on Cu_2O/Cu(111) while Nb_3O_7 is not, which is in agreement with our observed D_2O TPD results and proposed water dissociation mechanism. The results of repeated TPD runs on Nb_3O_5 are shown in Figure 7b. A high temperature peak

is still observed after the first run, but it is not as intense as in the first run. This can be explained in light of our proposed mechanism for water dissociation. During the first TPD run, the 2-propanol molecules react at the Lewis acid Nb=O sites, which then create Nb-OH-Nb Brønsted acid sites where more 2-propanol molecules can react. Therefore, the propene peak in the first TPD run has contributions from both Lewis and Brønsted acid sites. However, in the subsequent runs, the Lewis acid sites have already been used up, so only the Brønsted acid sites can contribute to the dehydration reaction, leading to a smaller propene TPD peak.

3.4. DFT Calculations of Water Dissociation on Nb_3O_7

We performed detailed DFT calculations of Nb_3O_7 (**1**) on Cu(111) and Cu_2O(111) to further our understanding of water dissociation on the cluster. First, we investigated the adsorption of a water molecule on Nb_3O_7 on Cu(111). We compared the energies of the systems with the water either adsorbed molecularly on a Nb cation or hydrogen bonded to a terminal oxygen, and found that the former is preferred by about 0.38 eV with E_{ads} of –0.56 eV. This result is consistent with the above proposed water dissociation mechanism, where the first step is the interaction of the water molecule with a Nb atom bonded to a terminal oxygen.

We subsequently calculated the reaction pathway for water dissociation, where the OH group from the water remains on the Nb atom and the dissociated H binds to a bridging oxygen. The calculated initial state with molecular adsorption of water, transition state, and the final state with the dissociated water are shown in Figure 8a. We found this dissociation reaction to be thermodynamically favorable (ΔE = –0.57 eV), and the reaction energy barrier was calculated to be fairly low at 0.28 eV. From comparison of Figure 3(b) and Figure 8(a), we note that water adsorption and dissociation breaks the terminal Nb=O double bond and

replaces it with two Nb-O single bonds in which the original terminal oxygen atom is now also bonded to a Cu atom on the surface. Hence, the formal bond order of the Nb cation at the active site is not changed and the charge distribution at the Nb cation is also not likely to be altered significantly. This expectation is consistent with a Bader charge analysis which finds that the Nb cation at the dissociation site loses only about 0.3e compared to its initial state without any water, and with our XPS results which show no significant changes before and after water dissociation.

We also considered water adsorption at the cluster-Cu(111) interface, where the O atom of the water molecule was bonded to a Cu atom and one of the H atoms formed a hydrogen bond with a terminal O atom of the cluster (optimized adsorption structure shown in Figure S6 in SI). The water adsorption energy was slightly lower in this case at –0.69 eV, but water dissociation from this adsorption site was endothermic due to the low stability of OH species on Cu(111).

Similar reaction pathway calculations were performed for Nb_3O_7 on a bulk terminated $Cu_2O(111)$ surface as a simplified model for the Cu_2O/Cu(111) oxide film (Figure 8b). Previous STM studies have shown that the "44" structure of the Cu_2O film formed by the oxidation procedure used in this work is structurally similar to the $Cu_2O(111)$ termination of the bulk oxide.[34] In this case, the calculations show that even though water dissociation is predicted to be slightly exothermic (ΔE = –0.15 eV), the energy barrier is substantially higher (E_a = 1.59 eV), and therefore dissociation is unlikely except at significantly higher temperatures. Additionally, all of the terminal Nb=O groups are lost to oxygen interactions with Cu atoms in the substrate even prior to water adsorption. These results are consistent with our experimental results, which showed that Nb_3O_7 was active toward water dissociation on Cu(111) but not on Cu_2O/Cu(111), and with our proposed water dissociation mechanism where the Nb=O group plays an important role. However, care must be taken when drawing

conclusions from calculations based on the bulk $Cu_2O(111)$ surface. Previous experimental and theoretical studies have shown that the electronic properties of nanoclusters can change depending on whether they are bonded to a bulk oxide surface or an ultrathin oxide film deposited on a metal substrate, due to electron transfer from the metal to the cluster through the oxide film.[67-69] In our case, Bader analysis indicates that more electrons are transferred to Nb_3O_7 on Cu(111) than on $Cu_2O(111)$ (+0.18e vs. +0.10e), with an average of 0.14 more electrons on each Nb cation in the cluster on Cu(111). Since Nb_3O_7 on Cu(111) is active for water dissociation but not on the Cu_2O film, the calculations suggest that the increased reduction of the Nb centers is responsible for making water dissociation more favorable. Qualitatively, this might be expected since electrons are needed for back-donation to the antibonding orbitals of the water molecule for it to dissociate and form stable OH species. However, this partial reduction via deposition on Cu(111) compared to that on Cu_2O/Cu(111) is at odds with our experimental 2PPE and XPS results, which point to greater electron transfer to the Nb_3O_7 cluster when deposited on Cu_2O/Cu(111). Further calculations on a Cu_2O film are required to determine whether the bulk $Cu_2O(111)$ serves as an adequate model for the ultrathin Cu_2O film, especially in describing charge transfer to surface species (clusters or adsorbates) that are of interest to heterogeneous catalysis.

4. Summary

We have used a combination of 2PPE, XPS, and DFT calculations to investigate the electronic interactions between size-selected Nb oxide clusters (Nb_3O_5, Nb_3O_7, Nb_4O_7, and Nb_4O_{10}) and their support of either Cu(111) or Cu_2O/Cu(111). For all of the studied systems, the work function increased with cluster coverage, resulting in interfacial dipole moments (μ) with the positive end pointing into the surface. We observed two intuitively reasonable trends: 1) μ is smaller for the reduced clusters compared to their fully oxidized counterparts, and 2) μ

is smaller for the clusters with less metal centers. An analysis of the relative contributions of charge transfer and the intrinsic cluster dipole moment to μ in the Cu(111) systems using DFT showed that while Cu(111) donates electrons to the fully oxidized clusters, Cu(111) receives electrons from the reduced clusters, and therefore the intrinsic cluster dipole moment is the major component of μ for the reduced clusters. The experimentally derived magnitude of μ was much greater on Cu_2O/Cu(111) than on Cu(111), suggesting greater electronic interactions between the clusters and the oxide film. Our XPS results of the Nb 3d region also showed clear changes when the clusters were deposited on Cu_2O/Cu(111) compared to on Cu(111).

The reactivity of all the Nb cluster systems toward water dissociation was studied by D_2O TPD experiments in which the desorbing D_2 molecules after recombination of the D atoms from dissociated D_2O were monitored. All systems exhibited activity except for the fully oxidized clusters deposited on Cu_2O/Cu(111). By correlating the TPD results with the XPS Nb cation charge state distributions and DFT calculated structures, it was possible to show that all the reactive systems contained terminal Nb=O oxo groups nominally associated with the presence of Nb^{5+} cations. A terminal Nb=O group is commonly considered to be a Lewis acid site and can interact with a water molecule. Therefore, we proposed a water dissociation mechanism in which the water molecules initially adsorb and dissociate at these Lewis acid sites. This initial phase of water dissociation is thought to create Brønsted acid sites, which can lead to further water dissociation. Our 2-propanol TPD results confirmed that the system active toward water dissociation, i.e., reduced Nb_3O_5 on Cu_2O/Cu(111), was indeed acidic, exhibiting dehydration of 2-propanol to propene, while the fully oxidized Nb_3O_7 on Cu_2O/Cu(111) did not exhibit dehydration.

The DFT-calculated energetics of water adsorption and dissociation on Nb_3O_7 on Cu(111) agree well with our experimental results. Water dissociation is thermodynamically

favored and the reaction barrier is relatively low. For Nb_3O_7 on the bulk terminated $Cu_2O(111)$ surface, the calculated barrier for water dissociation is much higher, which is consistent with the lack of observed activity for water dissociation. However, Bader analysis showed that the Nb cations in the cluster on Cu(111) are more reduced compared to on the $Cu_2O(111)$ surface. The latter is inconsistent with the experimental work function shifts (2PPE) and the Nb cation oxidation state distributions (XPS) which indicate electron transfer to the clusters when deposited on the $Cu_2O/Cu(111)$ surface. While having a strong Lewis acid center (terminal Nb=O groups) appears to be a key factor for catalyzing water dissociation, charge transfer and metal reducibility may also play a role because electrons are needed for back-donation to the water molecule to induce dissociation. Taking a closer look at the changes in interfacial charge transfer and the resulting activity toward water dissociation as a function of Cu oxide film thickness would be of great interest for WGS catalysis in the future.

Associated Content

Supporting Information

DFT-calculated adsorption structures of Nb_3O_x clusters on $Cu_2O(111)$, experimentally derived interfacial dipole moment values of the Nb oxide clusters on $Cu_2O/Cu(111)$, D_2O TPD results of a pre-annealed sample of Nb_3O_5 on Cu(111) compared to a normal TPD experiment, D_2O TPD results of Nb_4O_x clusters on Cu(111), Nb 3d XPS spectra and $3d_{5/2}$ peak parameters of Nb_3O_x clusters on Cu(111) and $Cu_2O/Cu(111)$ before and after D_2O TPD experiments, Nb 3d XPS spectra of Nb_3O_5 on Cu(111) before and after pre-annealing and conducting D_2O TPD experiments, and DFT-calculated structure of a water molecule adsorbed at the Nb_3O_7-Cu(111) interface. This material is available free of charge via the Internet at http://pubs.acs.org.

Acknowledgements

This work was supported by the U.S. Department of Energy, Office of Science, Office of Basic Energy Sciences under Contract No. DE-AC02-98CH10086. The DFT calculations were performed using computational resources at the Center for Functional Nanomaterials which is a DOE Office of Science User Facility located at Brookhaven National Laboratory. MN graciously acknowledges Prof. Sibener's guidance and support throughout her graduate studies at the University of Chicago.

References

(1) Amadeo, N. E.; Laborde, M. A. Hydrogen-Production from the Low-Temperature Water-Gas Shift Reaction - Kinetics and Simulation of the Industrial Reactor. *Int. J. Hydrogen Energy* **1995**, *20*, 949-956.

(2) Rhodes, C.; Hutchings, G. J.; Ward, A. M. Water-Gas Shift Reaction - Finding the Mechanistic Boundary. *Catal. Today* **1995**, *23*, 43-58.

(3) Choi, Y.; Stenger, H. G. Water Gas Shift Reaction Kinetics and Reactor Modeling for Fuel Cell Grade Hydrogen. *J. Power Sources* **2003**, *124*, 432-439.

(4) Shelef, M.; Gandhi, H. S. Ammonia Formation in Catalytic Reduction of Nitric-Oxide. 3. Role of Water Gas Shift, Reduction by Hydrocarbons, and Steam Reforming. *Ind. Eng. Chem. Prod. Res. Dev.* **1974**, *13*, 80-84.

(5) Ruettinger, W.; Ilinich, O.; Farrauto, R. J. A New Generation of Water Gas Shift Catalysts for Fuel Cell Applications. *J. Power Sources* **2003**, *118*, 61-65.

(6) Liu, X. M.; Lu, G. Q.; Yan, Z. F.; Beltramini, J. Recent Advances in Catalysts for Methanol Synthesis via Hydrogenation of CO and CO_2. *Ind. Eng. Chem. Res.* **2003**, *42*, 6518-6530.

(7) Rodriguez, J. A.; Liu, P.; Wang, X.; Wen, W.; Hanson, J.; Hrbek, J.; Perez, M.; Evans, J. Water-Gas Shift Activity of Cu Surfaces and Cu Nanoparticles Supported on Metal Oxides. *Catal. Today* **2009**, *143*, 45-50.

(8) Fernandez-Garcia, M.; Martinez-Arias, A.; Hanson, J. C.; Rodriguez, J. A. Nanostructured Oxides in Chemistry: Characterization and Properties. *Chem. Rev.* **2004**, *104*, 4063-4104.

(9) Rodriguez, J. A.; Hrbek, J. Inverse Oxide/Metal Catalysts: A Versatile Approach for Activity Tests and Mechanistic Studies. *Surf. Sci.* **2010**, *604*, 241-244.

(10) Yang, Y.; Zhou, J.; Nakayama, M.; Nie, L.; Liu, P.; White, M. G. Surface Dipoles and Electron Transfer at the Metal Oxide–Metal Interface: A 2PPE Study of Size-Selected Metal Oxide Clusters Supported on Cu(111). *J. Phys. Chem. C* **2014**, *118*, 13697-13706.

(11) Liu, P. Water-Gas Shift Reaction on Oxide/Cu(111): Rational Catalyst Screening from Density Functional Theory. *J. Chem. Phys.* **2010**, *133*, 204705-204711.

(12) Vidal, A. B.; Liu, P. Density Functional Study of Water-Gas Shift Reaction on M_3O_{3x}/Cu(111). *Phys. Chem. Chem. Phys.* **2012**, *14*, 16626-16632.

(13) Rodriguez, J. A.; Graciani, J.; Evans, J.; Park, J. B.; Yang, F.; Stacchiola, D.; Senanayake, S. D.; Ma, S. G.; Perez, M.; Liu, P.; et al. Water-Gas Shift Reaction on a Highly Active Inverse CeOx/Cu(111) Catalyst: Unique Role of Ceria Nanoparticles. *Angew Chem Int Edit* **2009**, *48*, 8047-8050.

(14) Nowak, I.; Ziolek, M. Niobium Compounds: Preparation, Characterization, and Application in Heterogeneous Catalysis. *Chem. Rev.* **1999**, *99*, 3603-3624.

(15) Ziolek, M. Niobium-Containing Catalysts - The State of the Art. *Catal. Today* **2003**, *78*, 47-64.

(16) Tanabe, K. Catalytic Application of Niobium Compounds. *Catal. Today* **2003**, *78*, 65-77.

(17) Ushikubo, T. Recent Topics of Research and Development of Catalysis by Niobium and Tantalum Oxides. *Catal. Today* **2000**, *57*, 331-338.

(18) Jehng, J.-M.; Wachs, I. E. The Molecular Structures and Reactivity of Supported Niobium Oxide Catalysts. *Catal. Today* **1990**, *8*, 37-55.

(19) Pittman, R. M.; Bell, A. T. Raman Studies of the Structure of Nb_2O_5/TiO_2. *J. Phys. Chem.* **1993**, *97*, 12178-12185.

(20) Sobczak, I.; Goscianska, J.; Ziolek, M.; Grams, J.; Verrier, C.; Bazin, P.; Marie, O.; Daturi, M. WGS and Reforming Properties of NbMCM-41 Materials. *Catal. Today* **2006**, *114*, 281-286.

(21) Zhang, F. L.; Zheng, Q.; Wei, K. M.; Lin, X. Y.; Zhang, H. H.; Li, J. W.; Cao, Y. N. Improved Performance of Au/Fe_2O_3 Catalysts Promoted with ZrO_2 and Nb_2O_5 in the WGS Reaction under Hydrogen-Rich Conditions. *Catal. Lett.* **2006**, *108*, 131-136.

(22) Domen, K.; Kudo, A.; Shinozaki, A.; Tanaka, A.; Maruya, K.; Onishi, T. Photodecomposition of Water and Hydrogen Evolution from Aqueous Methanol Solution over Novel Niobate Photocatalysts. *J. Chem. Soc., Chem. Commun.* **1986**, 356-357.

(23) Maeda, K.; Eguchi, M.; Youngblood, W. J.; Mallouk, T. E. Niobium Oxide Nanoscrolls as Building Blocks for Dye-Sensitized Hydrogen Production from Water under Visible Light Irradiation. *Chem. Mater.* **2008**, *20*, 6770-6778.

(24) Gokhale, A. A.; Dumesic, J. A.; Mavrikakis, M. On the Mechanism of Low-Temperature Water Gas Shift Reaction on Copper. *J. Am. Chem. Soc.* **2008**, *130*, 1402-1414.

(25) Zemski, K. A.; Justes, D. R.; Castleman, A. W. Studies of Metal Oxide Clusters: Elucidating Reactive Sites Responsible for the Activity of Transition Metal Oxide Catalysts. *J. Phys. Chem. B* **2002**, *106*, 6136-6148.

(26) Fielicke, A.; Meijer, G.; von Helden, G. Infrared Spectroscopy of Niobium Oxide Cluster Cations in a Molecular Beam: Identifying the Cluster Structures. *J. Am. Chem. Soc.* **2003**, *125*, 3659-3667.

(27) Dong, F.; Heinbuch, S.; He, S. G.; Xie, Y.; Rocca, J. J.; Bernstein, E. R. Formation and Distribution of Neutral Vanadium, Niobium, and Tantalum Oxide Clusters: Single Photon Ionization at 26.5 eV. *J. Chem. Phys.* **2006**, *125*, 164318-164325.

(28) Zhai, H. J.; Zhang, X. H.; Chen, W. J.; Huang, X.; Wang, L. S. Stoichiometric and Oxygen-Rich $M_2O_n^-$ and M_2O_n (M = Nb, Ta; n=5-7) Clusters: Molecular Models for Oxygen Radicals, Diradicals, and Superoxides. *J. Am. Chem. Soc.* **2011**, *133*, 3085-3094.

(29) Jackson, P.; Fisher, K. J.; Willett, G. D. The Catalytic Activation of Primary Alcohols on Niobium Oxide Surfaces Unraveled: The Gas Phase Reactions of Nb_xO_y- Clusters with Methanol and Ethanol. *Chem. Phys.* **2000**, *262*, 179-187.

(30) Zhai, H. J.; Dobler, J.; Sauer, J.; Wang, L. S. Probing the Electronic Structure of Early Transition-Metal Oxide Clusters: Polyhedral Cages of $(V_2O_5)_n^-$ (n = 2-4) and $(M_2O_5)_2^-$ (M = Nb, Ta). *J. Am. Chem. Soc.* **2007**, *129*, 13270-13276.

(31) Zemski, K. A.; Justes, D. R.; Bell, R. C.; Castleman, A. W. Reactions of Niobium and Tantalum Oxide Cluster Cations and Anions with n-Butane. *J. Phys. Chem. A* **2001**, *105*, 4410-4417.

(32) Deng, H. T.; Kerns, K. P.; Castleman, A. W. Formation, Structures, and Reactivities of Niobium Oxide Cluster Ions. *J. Phys. Chem.* **1996**, *100*, 13386-13392.

(33) Lightstone, J. M.; Patterson, M. J.; Liu, P.; White, M. G. Gas-Phase Reactivity of the $Ti_8C_{12}^+$ Met-car with Triatomic Sulfur-Containing Molecules: CS_2, SCO, and SO_2. *J. Phys. Chem. A* **2006**, *110*, 3505-3513.

(34) Yang, F.; Choi, Y. M.; Liu, P.; Hrbek, J.; Rodriguez, J. A. Autocatalytic Reduction of a Cu_2O/Cu(111) Surface by CO: STM, XPS, and DFT Studies. *J. Phys. Chem. C* **2010**, *114*, 17042-17050.

(35) Matsumoto, T.; Bennett, R. A.; Stone, P.; Yamada, T.; Domen, K.; Bowker, M. Scanning Tunneling Microscopy Studies of Oxygen Adsorption on Cu(111). *Surf. Sci.* **2001**, *471*, 225-245.

(36) Jensen, F.; Besenbacher, F.; Laegsgaard, E.; Stensgaard, I. Oxidation of Cu(111) - 2 New Oxygen Induced Reconstructions. *Surf. Sci.* **1991**, *259*, L774-L780.

(37) Jensen, F.; Besenbacher, F.; Stensgaard, I. 2 New Oxygen Induced Reconstructions on Cu(111). *Surf. Sci.* **1992**, *269*, 400-404.

(38) Soon, A.; Todorova, M.; Delley, B.; Stampfl, C. Oxygen Adsorption and Stability of Surface Oxides on Cu(111): A First-Principles Investigation. *Phys. Rev. B* **2006**, *73*, 165424-165435.

(39) Zhou, J.; Yang, Y. X.; Liu, P.; Camillone, N.; White, M. G. Electronic Structure of the Thiophene/Au(111) Interface Probed by Two-Photon Photoemission. *J. Phys. Chem. C* **2010**, *114*, 13670-13677.

(40) Seah, M. P.; Gilmore, L. S.; Beamson, G. XPS: Binding Energy Calibration of Electron Spectrometers 5 - Re-Evaluation of the Reference Energies. *Surf. Interface Anal.* **1998**, *26*, 642-649.

(41) Ghijsen, J.; Tjeng, L. H.; Vanelp, J.; Eskes, H.; Westerink, J.; Sawatzky, G. A.; Czyzyk, M. T. Electronic Structure of Cu_2O and CuO. *Phys. Rev. B* **1988**, *38*, 11322-11330.

(42) Kresse, G.; Furthmuller, J. Efficient Iterative Schemes for ab initio Total-Energy Calculations Using a Plane-Wave Basis Set. *Phys. Rev. B* **1996**, *54*, 11169-11186.

(43) Kresse, G.; Furthmuller, J. Efficiency of Ab-Initio Total Energy Calculations for Metals and Semiconductors Using a Plane-Wave Basis Set. *Comput. Mater. Sci.* **1996**, *6*, 15-50.

(44) Kresse, G.; Hafner, J. Ab initio Molecular-Dynamics for Liquid-Metals. *Phys. Rev. B* **1993**, *47*, 558-561.

(45) Perdew, J. P.; Chevary, J. A.; Vosko, S. H.; Jackson, K. A.; Pederson, M. R.; Singh, D. J.; Fiolhais, C. Atoms, Molecules, Solids, and Surfaces - Applications of the Generalized Gradient Approximation for Exchange and Correlation. *Phys. Rev. B* **1992**, *46*, 6671-6687.

(46) Kresse, G.; Joubert, D. From Ultrasoft Pseudopotentials to the Projector Augmented-Wave Method. *Phys. Rev. B* **1999**, *59*, 1758-1775.

(47) Monkhorst, H. J.; Pack, J. D. Special Points for Brillouin-Zone Integrations. *Phys. Rev. B* **1976**, *13*, 5188-5192.

(48) Henkelman, G.; Arnaldsson, A.; Jonsson, H. A Fast and Robust Algorithm for Bader Decomposition of Charge Density. *Comput. Mater. Sci.* **2006**, *36*, 354-360.

(49) Bader, R. F. W.; Beddall, P. M. Virial Field Relationship for Molecular Charge Distributions and Spatial Partitioning of Molecular Properties. *J. Chem. Phys.* **1972**, *56*, 3320-3329.

(50) Henkelman, G.; Uberuaga, B. P.; Jonsson, H. A Climbing Image Nudged Elastic Band Method for Finding Saddle Points and Minimum Energy Paths. *J. Chem. Phys.* **2000**, *113*, 9901-9904.

(51) Mills, G.; Jonsson, H.; Schenter, G. K. Reversible Work Transition-State Theory - Application to Dissociative Adsorption of Hydrogen. *Surf. Sci.* **1995**, *324*, 305-337.

(52) Hagen, S.; Leyssner, F.; Nandi, D.; Wolf, M.; Tegeder, P. Reversible Switching of tetra-tert-butyl-azobenzene on a Au(111) Surface Induced by Light and Thermal Activation. *Chem. Phys. Lett.* **2007**, *444*, 85-90.

(53) Wang, H. F.; Dutton, G.; Zhu, X. Y. Electronic Structure at Organic/Metal Interfaces: Naphthalene/Cu(111). *J. Phys. Chem. B* **2000**, *104*, 10332-10338.

(54) Wei, W.; White, J. M. Two-Photon Photoemission Spectroscopy: Atomic Oxygen on Cu(111) and Styrene on Oxygen Covered Cu(111). *Proc. SPIE* **2004**, *5513*, 157-164.

(55) Topping, J. On the Mutual Potential Energy of a Plane Network of Doublets. *Proc. R. Soc. London, Ser. A* **1927**, *114*, 67-72.

(56) Yates, J. T.; Klein, R.; Madey, T. E. Adsorption of Molecular Nitrogen by W(110) Plane. *Surf. Sci.* **1976**, *58*, 469-478.

(57) Pivetta, M.; Patthey, F.; Schneider, W. D.; Delley, B. Surface Distribution of Cu Adatoms Deduced from Work Function Measurements. *Phys. Rev. B* **2002**, *65*, 045417-045421.

(58) Dacca, A.; Gemme, G.; Mattera, L.; Parodi, R. XPS analysis of the surface composition of niobium for superconducting RF cavities. *Appl. Surf. Sci.* **1998**, *126*, 219-230.

(59) Prada, S.; Martinez, U.; Pacchioni, G. Work Function Changes Induced by Deposition of Ultrathin Dielectric Films on Metals: A Theoretical Analysis. *Phys. Rev. B* **2008**, *78*, 235423-235430.

(60) Delheusy, M. X-ray Investigation of Nb/O Interfaces. University of Paris-Sud, University of Stuttgart, 2008.

(61) Atuchin, V. V.; Kalabin, I. E.; Kesler, V. G.; Pervukhina, N. V. Nb 3d and O 1s Core Levels and Chemical Bonding In Niobates. *J. Electron Spectrosc. Relat. Phenom.* **2005**, *142*, 129-134.

(62) Mason, M. G. Electronic-Structure of Supported Small Metal-Clusters. *Phys. Rev. B* **1983**, *27*, 748-762.

(63) Hota, M. K.; Bera, M. K.; Verma, S.; Maiti, C. K. Studies on Switching Mechanisms in Pd-Nanodot Embedded Nb_2O_5 Memristors Using Scanning Tunneling Microscopy. *Thin Solid Films* **2012**, *520*, 6648-6652.

(64) Razinkin, A. S.; Shalaeva, E. V.; Kuznetsov, M. V. Photoelectron Spectroscopy and Diffraction of NbO_x/Nb(110) Surface. *Phys. Met. Metallogr.* **2008**, *106*, 56-66.

(65) Sterrer, M.; Risse, T.; Pozzoni, U. M.; Giordano, L.; Heyde, M.; Rust, H. P.; Pacchioni, G.; Freund, H. J. Control of the Charge State of Metal Atoms on Thin MgO Films. *Phys. Rev. Lett.* **2007**, *98*, 096107-096110.

(66) Freund, H. J.; Pacchioni, G. Oxide Ultra-Thin Films on Metals: New Materials for the Design of Supported Metal Catalysts. *Chem. Soc. Rev.* **2008**, *37*, 2224-2242.

(67) Zhou, J.; Zhou, J.; Camillone, N.; White, M. G. Electronic Charging of Non-Metallic Clusters: Size-Selected Mo_xS_y Clusters Supported on an Ultrathin Alumina Film on NiAl(110). *Phys. Chem. Chem. Phys.* **2012**, *14*, 8105-8110.

(68) Zhu, J.; Giordano, L.; Lin, S. J.; Fang, Z. X.; Li, Y.; Huang, X.; Zhang, Y. F.; Pacchioni, G. Tuning the Charge State of $(WO_3)_3$ Nanoclusters Deposited on MgO/Ag(001) Films. *J. Phys. Chem. C* **2012**, *116*, 17668-17675.

(69) Torelli, P.; Giordano, L.; Benedetti, S.; Luches, P.; Annese, E.; Valeri, S.; Pacchioni, G. X-ray Photoemission Study of the Charge State of Au Nanoparticles on Thin MgO/Fe(001) Films. *J. Phys. Chem. C* **2009**, *113*, 19957-19965.

(70) Sun, Q.; Fu, Y. C.; Yang, H. X.; Auroux, A.; Shen, J. Y. Dehydration of Methanol to Dimethyl Ether over Nb_2O_5 and $NbOPO_4$ Catalysts: Microcalorimetric and FT-IR Studies. *J. Mol. Catal. A: Chem.* **2007**, *275*, 183-193.

(71) Jehng, J. M.; Wachs, I. E. Molecular Structures of Supported Niobium Oxide Catalysts under in situ Conditions. *J. Phys. Chem.* **1991**, *95*, 7373-7379.

(72) Corma, A.; Xamena, F. X. L. I.; Prestipino, C.; Renz, M.; Valencia, S. Water Resistant, Catalytically Active Nb and Ta Isolated Lewis Acid Sites, Homogeneously Distributed by Direct Synthesis in a Beta Zeolite. *J. Phys. Chem. C* **2009**, *113*, 11306-11315.

(73) Xie, L.; Wang, D. H.; Zhong, C. M.; Guo, X. X.; Ushikubo, T.; Wada, K. The Preparation of and Water-Adsorption on Thin-Films of Niobium Oxide on Pt(111). *Surf. Sci.* **1994**, *320*, 62-76.

(74) Lee, E. L.; Wachs, I. E. In situ Spectroscopic Investigation of the Molecular and Electronic Structures of SiO_2 Supported Surface Metal Oxides. *J. Phys. Chem. C* **2007**, *111*, 14410-14425.

(75) Henderson, M. A. The Interaction of Water with Solid Surfaces: Fundamental Aspects Revisited. *Surf. Sci. Rep.* **2002**, *46*, 1-308.

(76) Takagaki, A.; Lu, D. L.; Kondo, J. N.; Hara, M.; Hayashi, S.; Domen, K. Exfoliated HNb_3O_8 Nanosheets as a Strong Protonic Solid Acid. *Chem. Mater.* **2005**, *17*, 2487-2489.

(77) Andersson, K.; Ketteler, G.; Bluhm, H.; Yamamoto, S.; Ogasawara, H.; Pettersson, L. G. M.; Salmeron, M.; Nilsson, A. Autocatalytic Water Dissociation on Cu(110) at Near Ambient Conditions. *J. Am. Chem. Soc.* **2008**, *130*, 2793-2797.

(78) Bange, K.; Grider, D. E.; Madey, T. E.; Sass, J. K. The Surface Chemistry of H_2O on Clean and Oxygen-Covered Cu(110). *Surf. Sci.* **1984**, *137*, 38-64.

(79) Kubota, J.; Kondo, J.; Domen, K.; Hirose, C. An IRAS Study of Hydroxyl Species (OD(a)) on Oxygen-Modified Cu(110) Surface. *Surf. Sci.* **1993**, *295*, 169-173.

(80) Sueyoshi, T.; Sasaki, T.; Iwasawa, Y. Oxygen Atoms on Cu(100) Formed at 100 K, Active for CO Oxidation and Water-Hydrogen Abstraction, Characterized by HREELS and TPD. *J. Phys. Chem. B* **1997**, *101*, 4648-4655.

(81) Lee, J.; Sorescu, D. C.; Jordan, K. D.; Yates, J. T. Hydroxyl Chain Formation on the Cu(110) Surface: Watching Water Dissociation. *J. Phys. Chem. C* **2008**, *112*, 17672-17677.

(82) The partially oxygen covered surface was prepared by exposing the Cu(111) surface to 100 L of O_2 gas at a surface temperature of 400 K.

(83) Wagner, M.; Surnev, S.; Ramsey, M. G.; Barcaro, G.; Sementa, L.; Negreiros, F. R.; Fortunelli, A.; Dohnalek, Z.; Netzer, F. P. Structure and Bonding of Tungsten Oxide Clusters on Nanostructured Cu-O Surfaces. *J. Phys. Chem. C* **2011**, *115*, 23480-23487.

(84) Ai, M. Oxidation Activity and Acid-Base Properties of V_2O_5-Based Binary Catalysts. *Bull. Chem. Soc. Jpn.* **1977**, *50*, 2579-2583.

(85) Gervasini, A.; Auroux, A. Acidity and Basicity of Metal-Oxide Surfaces. 2. Determination by Catalytic Decomposition of Isopropanol. *J. Catal.* **1991**, *131*, 190-198.

(86) Kim, Y. K.; Rousseau, R.; Kay, B. D.; White, J. M.; Dohnalek, Z. Catalytic Dehydration of 2-Propanol on $(WO_3)_3$ Clusters on TiO_2(110). *J. Am. Chem. Soc.* **2008**, *130*, 5059-5061.

(87) Fang, Z. T.; Li, Z. J.; Kelley, M. S.; Kay, B. D.; Li, S. G.; Hennigan, J. M.; Rousseau, R.; Dohnalek, Z.; Dixon, D. A. Oxidation, Reduction, and Condensation of Alcohols over $(MO_3)_3$ (M = Mo, W) Nanoclusters. *J. Phys. Chem. C* **2014**, *118*, 22620-22634.

Table 1. Calculated shadow area in the plane of the surface, interfacial dipole (μ) obtained from experiment, and calculated Bader charge of the Nb oxide clusters on Cu(111)

	Nb_3O_5	Nb_3O_7	Nb_4O_7	Nb_4O_{10}
Shadow area ($Å^2$)	38.0 (**1**) 38.5 (**2**)	44.8 (**1**) 43.8 (**2**)	34.0	41.5
μ (D)	–0.40	–0.83	–0.70	–2.14
Bader charge (e)	–0.91 (**1**) –0.46 (**2**)	+0.18 (**1**) +0.35 (**2**)	–0.55	+1.34

Table 2. Summary of XPS peak positions and their FWHM values (in eV) in the Nb 3d region, and the percentage of Nb in the +5 oxidation state (%Nb^{5+}) as determined from the peak areas

		Nb^{5+}			Nb^{4+}			Nb^{3+}			
		$3d_{3/2}$	$3d_{5/2}$	FWHM	$3d_{3/2}$	$3d_{5/2}$	FWHM	$3d_{3/2}$	$3d_{5/2}$	FWHM	$\%Nb^{5+}$
on Cu(111)	Nb_3O_5	210.6	207.9	2.5	—	—	—	207.9	205.3	2.2	49.6
	Nb_3O_7	210.6	207.9	2.5	209.2	206.4	2.5	—	—	—	88.5
	Nb_4O_7	210.6	207.9	2.5	—	—	—	207.9	205.2	2.2	53.0
	Nb_4O_{10}	210.6	207.9	2.3	—	—	—	—	—	—	100
on Cu_2O	Nb_3O_5	210.6	207.9	2.4	209.5	206.7	2.1	—	—	—	55.8
	Nb_3O_7	210.7	207.9	2.1	209.6	206.8	1.8	—	—	—	25.3
	Nb_4O_7	210.7	207.9	2.0	209.4	206.6	1.7	—	—	—	38.3
	Nb_4O_{10}	210.6	207.9	2.1	209.4	206.6	1.8	—	—	—	15.3

Figure Captions:

Figure 1. A sample mass distribution of niobium oxide clusters produced by DC magnetron sputtering. The peaks of the clusters studied in this work are indicated by arrows.

Figure 2. Subsets of 2PPE spectra taken on Nb_3O_7 clusters (a) on Cu(111) and (b) on a Cu_2O film on Cu(111) at different local cluster coverages. The first image state and surface state of Cu(111) are labeled as IS_1 and SS, respectively. These states are suppressed as more clusters are deposited on the surface or when an oxide film is present. A feature from the Cu 3d band is also observed (Cu 3d), as well as a feature attributed to an unoccupied state on the Cu_2O/Cu(111) system. The low-energy cutoff energy corresponds to the work function of the system, which increases with increasing cluster coverage but at different rates on the two substrates.

Figure 3. Side and top views of the DFT-calculated adsorption structures of niobium oxide clusters on Cu(111): (a) Nb_3O_5, (b) Nb_3O_7, (c) Nb_4O_7, and (d) Nb_4O_{10}. For Nb_3O_5 and Nb_3O_7, an additional structure (structures **2**) within 0.5 eV of our lowest calculated energy structure (structures **1**) was found. The color scheme is as follows: blue-green, Nb; red, O; and blue, Cu.

Figure 4. Plots of the work function shift as measured by 2PPE versus the local niobium oxide cluster coverage on (a) Cu(111) and (b) Cu_2O/Cu(111). The solid lines are the results of the least-square fitting of the data to the Topping model. The work function shift is much greater and the depolarization effect more apparent for the clusters on Cu_2O/Cu(111).

Figure 5. XPS spectra of the Nb 3d region with peak fittings for the niobium oxide clusters on Cu(111) and Cu_2O/Cu(111): (a) Nb_3O_5, (b) Nb_3O_7, (c) Nb_4O_7, and (d) Nb_4O_{10}. All spectra are taken on samples with an average cluster coverage of 0.3 ML. For each panel, the top spectrum is taken on Cu(111) and the bottom on Cu_2O/Cu(111). It can be seen that the

spectra change significantly between the two substrates. The peaks from the different oxidation states are color-coded for clarity: red, +5; blue, +4; and green, +3. The gray dots are the raw data, and the solid black line running through them is the sum of the fitted peaks.

Figure 6. (a) The D_2 signal from D_2O TPD experiments for the niobium oxide clusters on Cu(111). All of the clusters are active for water dissociation. (b) The D_2 signal from D_2O TPD experiments for the clusters on Cu_2O/Cu(111). Only the reduced clusters are active. For (a) and (b), data from the first TPD run of each experiment is shown. (c) The D_2 signal from three consecutive TPD runs for Nb_3O_7 on Cu(111). The signal increases after the first run. (d) The D_2O signal from three consecutive TPD runs for Nb_3O_7 on Cu(111). A shoulder appears above 300 K after the first run. All of the D_2O TPD experiments were conducted on samples with an average cluster coverage of 0.3 ML.

Figure 7. (a) The propene signal, monitored at 41 amu, from 2-propanol TPD experiments of Nb_3O_5 and Nb_3O_7 on Cu_2O/Cu(111). The spectrum from bare Cu_2O/Cu(111) is also shown as a reference. The initial peak near 200 K is from the desorption of physisorbed 2-propanol. The high-temperature peak around 460 K for Nb_3O_5 indicates that the cluster is active for the dehydration of 2-propanol on Cu_2O/Cu(111). The results for three consecutive TPD runs on Nb_3O_5 are shown in (b). The intensity of the high-temperature peak decreases after the first run. All of the 2-propanol TPD experiments were conducted on samples with an average cluster coverage of 0.15 ML.

Figure 8. The calculated initial state (IS), transition state (TS), and final state (FS) of the reaction pathway of water dissociation on Nb_3O_7 on (a) Cu(111) and (b) Cu_2O(111). The values in parentheses are the energies of each state relative to the sum of the energies of the optimized cluster/substrate system and an isolated water molecule. The energy of the initial state corresponds to the water adsorption energy. The activation energy (E_a) is taken as the energy difference between the transition and initial states, and it is much higher for (b). The

energy change of the reaction is the energy difference between the final and initial states, which is -0.57 eV for (a) and -0.15 eV for (b). The color scheme is as follows: blue-green, Nb; red, O of cluster; purple, O of substrate; and blue, Cu.

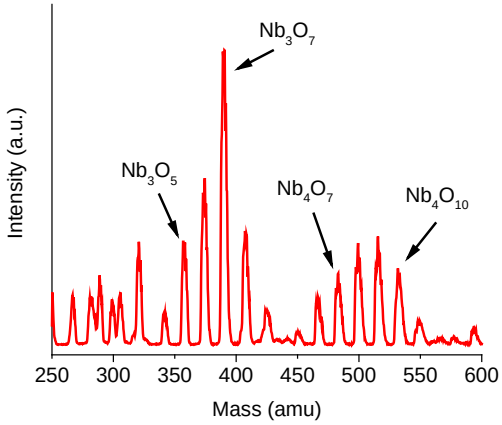
Nb3O7
Nb3O5
Nb4O7
Nb4O10
Intensity (a.u.)
250
300
350
400
450
500
550
600
Mass (amu)

Figure 1

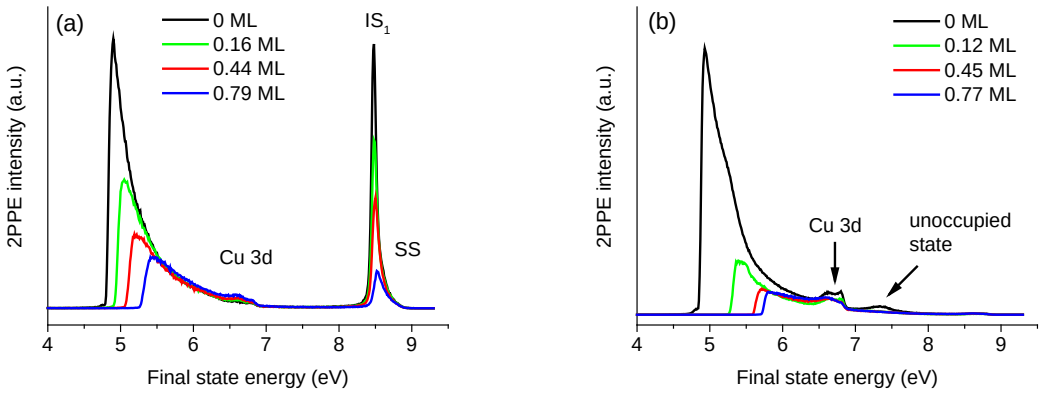
(a)
0 ML
0.16 ML
0.44 ML
0.79 ML
IS1
SS
Cu 3d
2PPE intensity (a.u.)
Final state energy (eV)
(b)
0 ML
0.12 ML
0.45 ML
0.77 ML
Cu 3d
unoccupied state
2PPE intensity (a.u.)
Final state energy (eV)

Figure 2

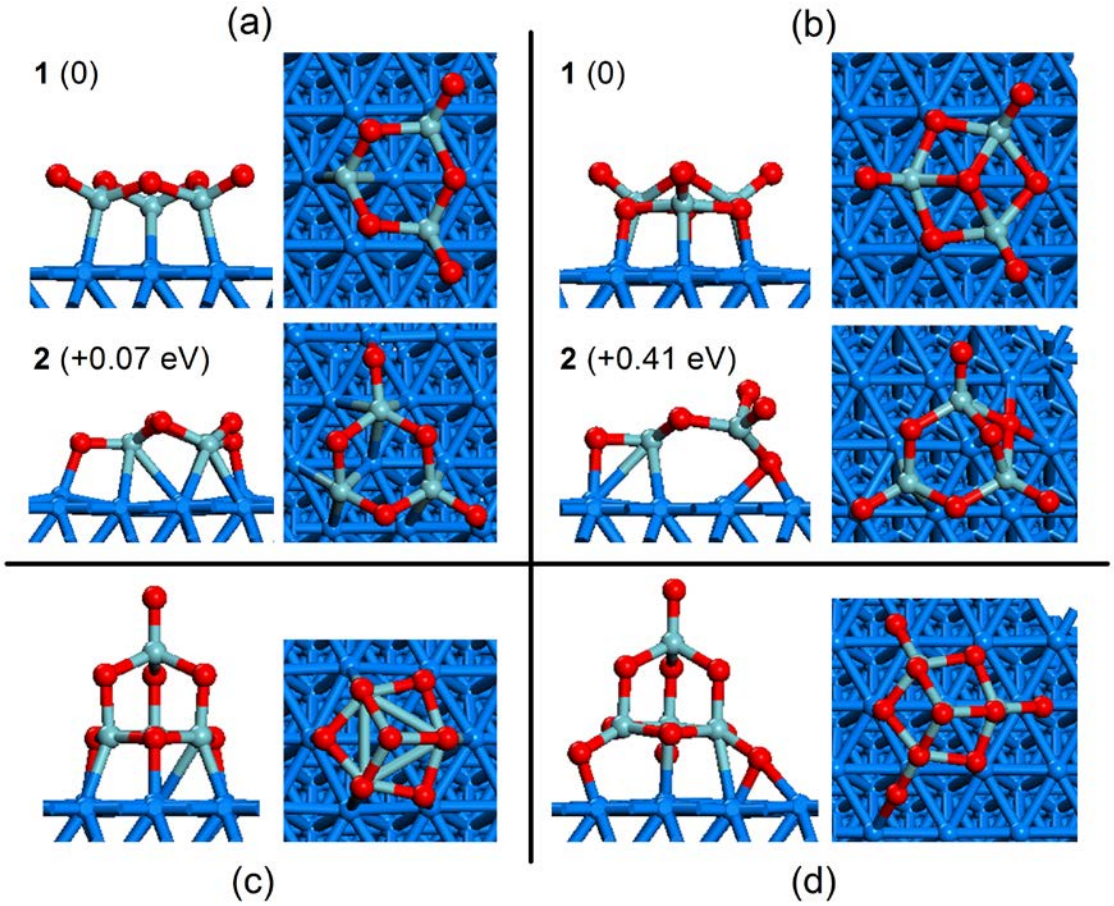

Figure 3

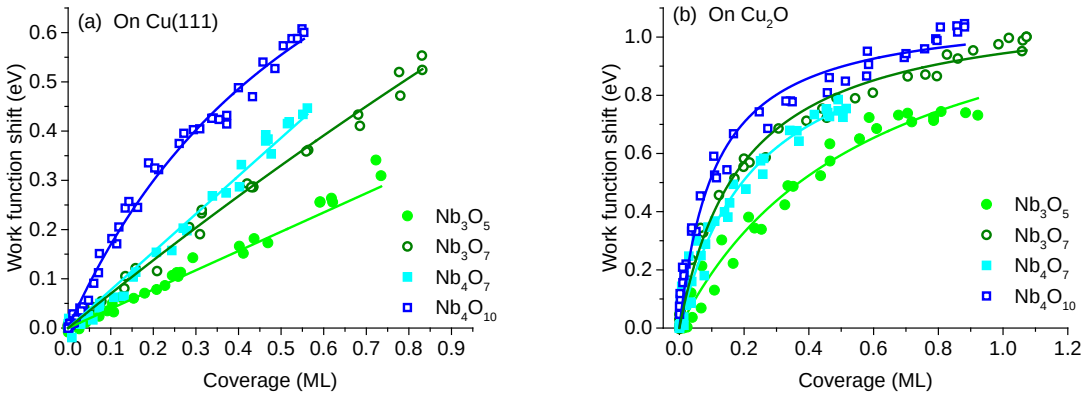
(a) On Cu(111)
Work function shift (eV)
Coverage (ML)
Nb3O5
Nb3O7
Nb4O7
Nb4O10
(b) On Cu2O
Work function shift (eV)
Coverage (ML)
Nb3O5
Nb3O7
Nb4O7
Nb4O10

Figure 4

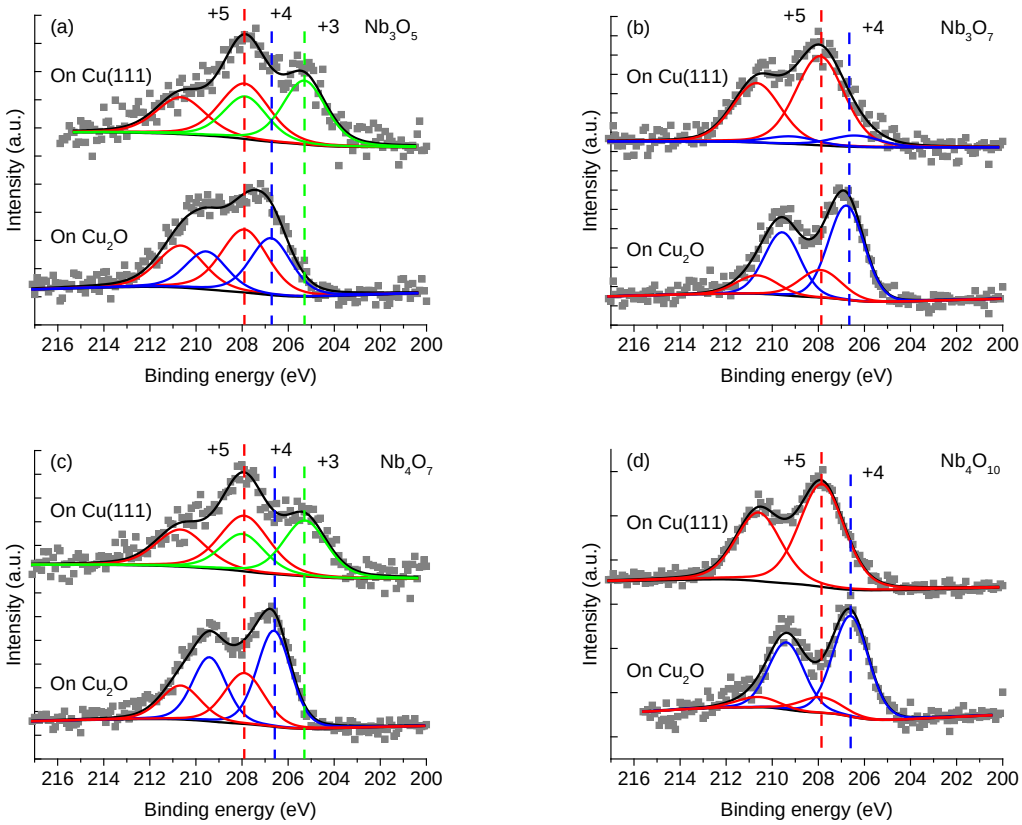
(a)
+5
+4
+3
Nb3O5
On Cu(111)
On Cu2O
Intensity (a.u.)
216 214 212 210 208 206 204 202 200
Binding energy (eV)
(b)
+5
+4
Nb3O7
On Cu(111)
On Cu2O
Intensity (a.u.)
216 214 212 210 208 206 204 202 200
Binding energy (eV)
(c)
+5
+4
+3
Nb4O7
On Cu(111)
On Cu2O
Intensity (a.u.)
216 214 212 210 208 206 204 202 200
Binding energy (eV)
(d)
+5
+4
Nb4O10
On Cu(111)
On Cu2O
Intensity (a.u.)
216 214 212 210 208 206 204 202 200
Binding energy (eV)

Figure 5

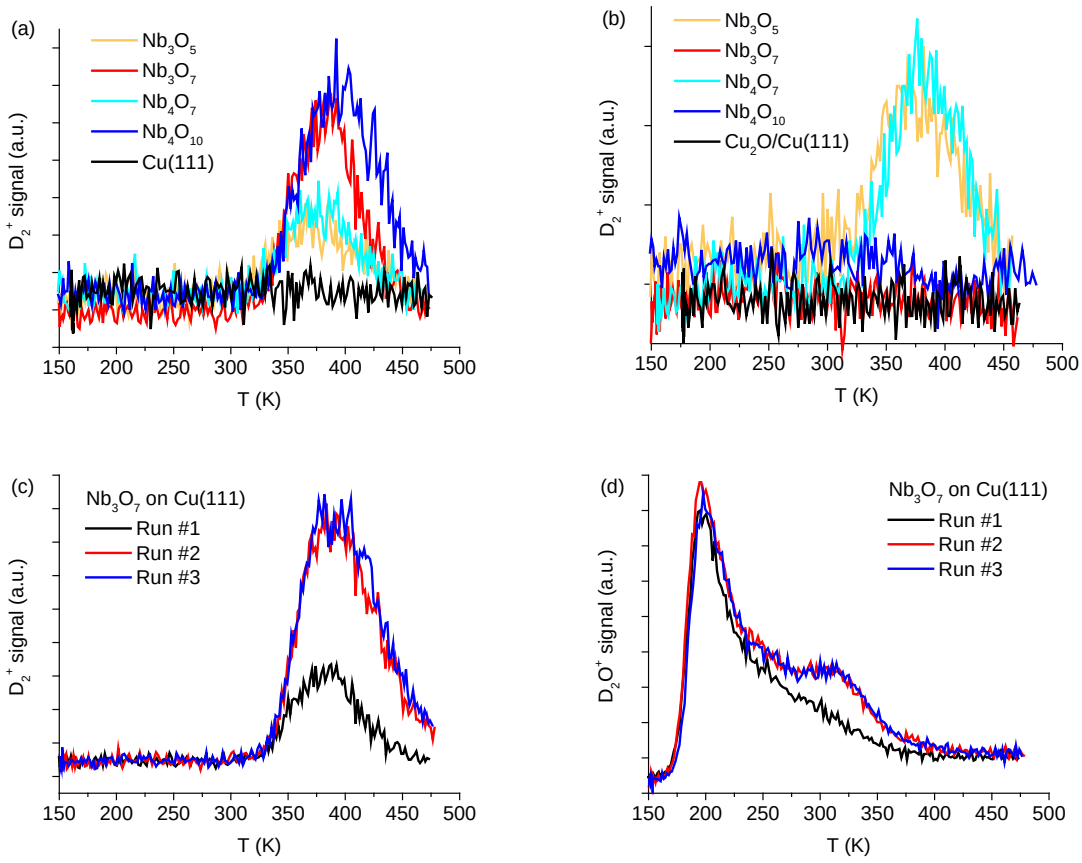
(a)
Nb3O5
Nb3O7
Nb4O7
Nb4O10
Cu(111)
D2+ signal (a.u.)
150 200 250 300 350 400 450 500
T (K)
(b)
Nb3O5
Nb3O7
Nb4O7
Nb4O10
Cu2O/Cu(111)
D2+ signal (a.u.)
150 200 250 300 350 400 450 500
T (K)
(c)
Nb3O7 on Cu(111)
Run #1
Run #2
Run #3
D2+ signal (a.u.)
150 200 250 300 350 400 450 500
T (K)
(d)
Nb3O7 on Cu(111)
Run #1
Run #2
Run #3
D2O+ signal (a.u.)
150 200 250 300 350 400 450 500
T (K)

Figure 6

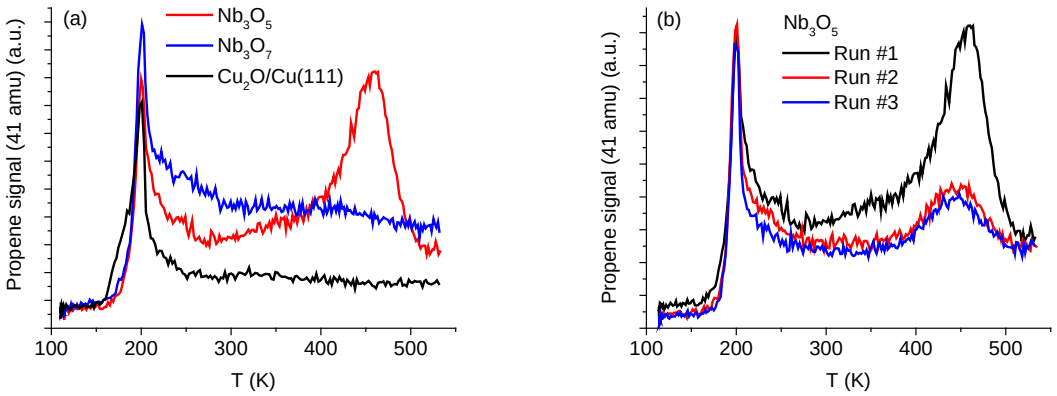
(a)
Nb3O5
Nb3O7
Cu2O/Cu(111)
Propene signal (41 amu) (a.u.)
100
200
300
400
500
T (K)
(b)
Nb3O5
Run #1
Run #2
Run #3
Propene signal (41 amu) (a.u.)
100
200
300
400
500
T (K)

Figure 7

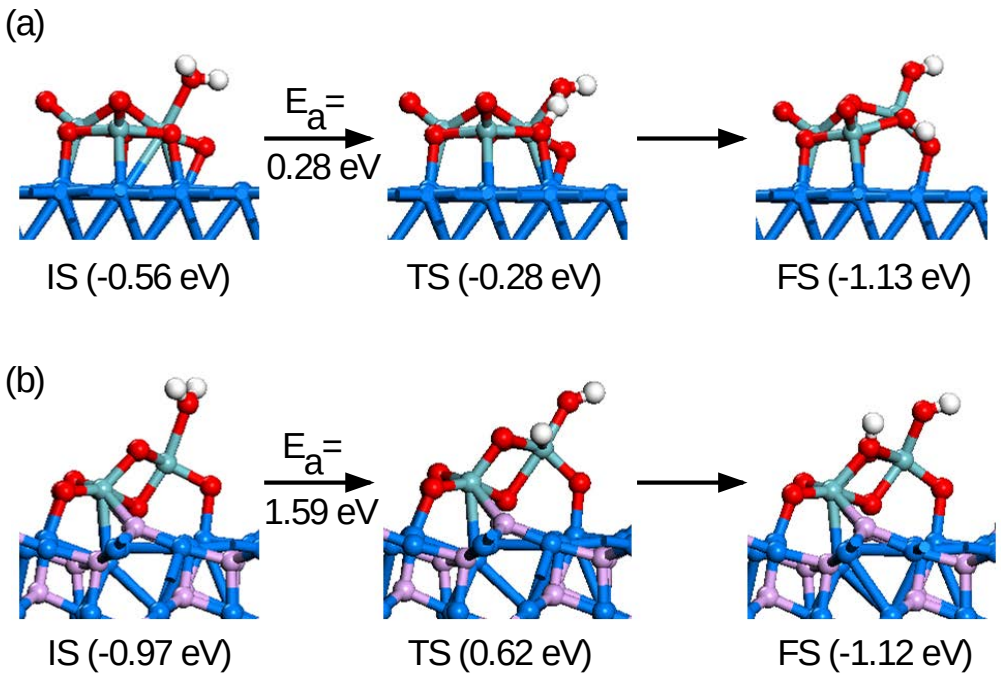
(a)
E_a=
0.28 eV
IS (-0.56 eV)
TS (-0.28 eV)
FS (-1.13 eV)
(b)
E_a=
1.59 eV
IS (-0.97 eV)
TS (0.62 eV)
FS (-1.12 eV)

Figure 8

TOC Graphic